# Sound in Curved Intakes

Edward J. Brambley[*], Nigel Peake[†]

*University of Cambridge, Cambridge CB3 0WA, UK*

**Military aircraft engine intakes are typically curved, the curvature and change in cross-section being significant but varying on a lengthscale far longer than a typical sound wavelength. This allows the use of the Method of Multiple Scales, as we presented at last year's conference. Here we further investigate this situation.**

**After a briefly recapping the (frequency-domain) Multiple Scales derivation from last year, we give an example of using this model to give time-domain results. For a relatively low-frequency pulse introduced at the downstream end of an RAE 2129 intake as a plane wave, the curvature and narrowing of the intake cause a peak pressure on the intake wall of 1.6 times the peak imposed pressure. This peak pressure is highly localized on the inside of a bend.**

**If a higher frequency comparable to the blade passing frequency is used, two upstream-propagating plane waves are supported by the intake, one localized on the inside of a bend and one on the outside. This phenomenon is investigated, and an explanation hazarded at the cause of the localization, by applying raytracing theory, at least for high frequencies. We give a simple algebraic expression for the parameters for which such localization can occur, and simple asymptotically-correct small-curvature formulae for these parameters.**

**In this paper, a wide range of results will be presented and explained, as well as preliminary developments of a nonlinear model for large-amplitude waves in curved intakes.**

## I.  Introduction

Many military aircraft engine intakes are strongly curved. Not only does the curved geometry cause sound to propagate differently from a straight intake, but also the inhomogeneity of the mean flow leads to refraction. For many military aircraft engine intakes, the curvature is significant and large, but varies on a lengthscale far longer than a typical sound wavelength. The diameter of the intake also varies slowly in this way. At last year's conference,[1] we presented a mathematical model based on the Method of Multiple Scales, and gave some preliminary numerical examples using this method. The effect of curvature and mean flow together was found to be dramatic; mode shapes became highly distorted from their straight-duct shapes, and some modes became concentrated on the inside or outside of the bend. Based on these preliminary results, we suggested that upstream-propagating modes are confined to the inside of a bend, while downstream-propagating modes are confined to the outside. However, the picture turns out to be more complicated.

In a number of cases, in particular buzzsaw noise or surge propagation, one is often interested in the development of coherent wave pulses, made up of several harmonics, for which it is useful to investigate the propagation of pulses in the time domain. After a brief review of the Multiple Scales approximation and restating the governing equations in section II, in section III we use this approximation to give some time-domain results of a wave pulse propagating through a standard reference duct geometry (the RAE 2129 inlet diffuser duct). In section IV we consider the localization behaviour mentioned above for the curved-duct equivalent of a plane wave. Finally, since buzzsaw noise or surge events are typically of large amplitude, in section V we present some preliminary nonlinear results for a pulse propagating through a two-dimensional version of the RAE 2129 intake.

---

[*]PhD student, Department of Applied Mathematics & Theoretical Physics, University of Cambridge, Centre for Mathematical Sciences, Wilberforce Road, Cambridge CB3 0WA, United Kingdom. AIAA member.

[†]Professor, Department of Applied Mathematics & Theoretical Physics, University of Cambridge, Centre for Mathematical Sciences, Wilberforce Road, Cambridge CB3 0WA, United Kingdom. AIAA member.

## II. Multiple Scales derivation

The derivation of this section mirrors that given at last year's conference,[1] and is included here for completeness, although here we are less general and consider only a hard-walled hollow duct. The Method of Multiple Scales we use is inspired by a similar application for a straight duct by Rienstra.[2]

### A. Steady Flow

We consider a duct whose centreline possesses nonzero curvature but zero torsion (i.e. the centreline lies in a plane). The duct has a circular cross-section in planes normal to the centreline. Let $s^*$ be the arc-length along the duct centreline ($^*$ denotes dimensional variables). Far upstream ($s^* \to -\infty$) the duct is assumed to be straight and of uniform outer radius $\ell^*$. The radii of the inner (and outer) walls and the centreline curvature then vary along the duct on the lengthscale $L^*$, so that the duct radius $a^*$ and the centreline curvature $\kappa^*$ are functions of $S \equiv s^*/L^*$. The requirement of slow variation along the axis is then equivalent to $\epsilon \equiv \ell^*/L^* \ll 1$. The duct carries a mean flow, which far upstream has uniform density $D_\infty^*$, speed $U_\infty^*$ and sound speed $C_\infty^*$. In what follows speeds are non-dimensionalized by $C_\infty^*$, densities by $D_\infty^*$, distances by $\ell^*$, times by $\ell^*/C_\infty^*$, and pressures by $(C_\infty^*)^2 D_\infty^*$. We introduce the duct-centred coordinate system $(s, r, \theta)$, where $r, \theta$ are polar coordinates in planes normal to the duct centreline, and $s$ is the arc-length along the centreline. The duct radius is $a(S)$ and the centreline curvature is $\kappa(S)$, where $S = \varepsilon s$ is the nondimensionalized slow coordinate over which the duct geometry varies.

The steady velocity in the duct is written $\boldsymbol{U} = U\boldsymbol{e_s} + V\boldsymbol{e_r} + W\boldsymbol{e_\theta}$, and it is assumed that all steady mean flow variables are functions of $r, \theta, S$, i.e. vary slowly down the duct. We assume an inviscid irrotational perfect gas with ratio of specific heats $\gamma$. We apply the steady continuity condition $\boldsymbol{\nabla}.(D\boldsymbol{U}) = 0$,

$$\frac{\varepsilon}{h_s}\frac{\partial}{\partial S}(DU) + \frac{1}{rh_s}\frac{\partial}{\partial r}(rh_s DV) + \frac{1}{rh_s}\frac{\partial}{\partial \theta}(h_s DW) = 0, \qquad h_s = 1 - \kappa(S)r\cos\theta$$

together with the condition for irrotational mean flow, $\boldsymbol{\nabla} \wedge \boldsymbol{U} = 0$,

$$\frac{1}{r}\frac{\partial}{\partial r}(rW) - \frac{1}{r}\frac{\partial V}{\partial \theta} = 0, \qquad \frac{1}{rh_s}\frac{\partial}{\partial \theta}(h_s U) - \frac{\varepsilon}{h_s}\frac{\partial W}{\partial S} = 0, \qquad \frac{\varepsilon}{h_s}\frac{\partial V}{\partial S} - \frac{1}{h_s}\frac{\partial}{\partial r}(h_s U) = 0,$$

and the irrotational form of Bernoulli's equation,

$$\frac{1}{2}U^2 + \frac{1}{\gamma - 1}D^{\gamma - 1} = H, \tag{1}$$

where the enthalpy $H = U_\infty^2/2 + 1/(\gamma - 1)$ is a constant determined at upstream infinity. The duct walls are considered perfectly hard and impenetrable, with the corresponding boundary conditions

$$V - \frac{\varepsilon}{h_s}\frac{\mathrm{d}a}{\mathrm{d}S}U = 0 \qquad \text{at } r = a(S). \tag{2}$$

We assume no leading-order potential swirl, so that $W$ vanishes to leading order. Putting all these assumptions together, we find that

$$D = D_0 + O(\varepsilon^2), \qquad U = U_0 + O(\varepsilon^2), \qquad V = \varepsilon V_1 + O(\varepsilon^3), \qquad W = \varepsilon W_1 + O(\varepsilon^3),$$

where

$$U_0(S, r, \theta) = \frac{U_\dagger(S)}{h_s(r, \theta, S)}, \qquad D_0 = \left[(\gamma - 1)\left(H - \frac{1}{2}U_0^2\right)\right]^{1/\gamma - 1}.$$

The quantity $U_\dagger$ may be found in terms of $U_\infty$ by applying conservation of mass at different axial locations,

$$\int_0^{2\pi}\int_0^a U_0 D_0 r\,\mathrm{d}r\,\mathrm{d}\theta = \pi U_\infty, \tag{3}$$

which can easily be solved numerically. Note that the mean velocity components in the plane of cross-section arise, in irrotational flow, from the slow variation of the duct, and are therefore $O(\varepsilon)$. In what follows it
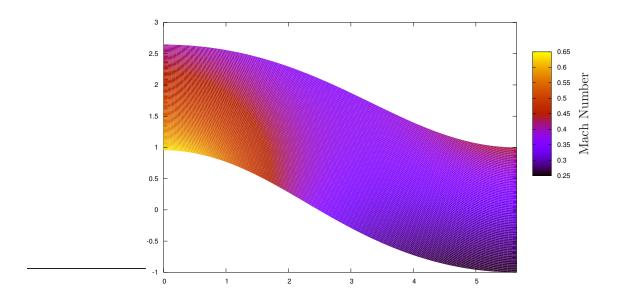
**Figure 1. A cross-section through the centreline of the RAE 2129 Inlet Diffuser intake, showing the steady-state flow with an inlet Mach number of $U_\infty = 0.5$. The flow is left to right, with the inlet lip on the left and the fan face on the right.**

turns out that the value of the radial velocity $V_1$ is only required on the walls, and can be found simply from the $O(\varepsilon)$ terms in the boundary condition (2). The value of the $O(\varepsilon)$ tangential velocity $W_1$ will not be required at all in our final answer for the unsteady flow.

One duct geometry we shall consider in particular is the RAE 2129 Inlet Diffuser duct, which is a much studied reference duct geometry.[3] A cross-section along the RAE 2129 duct centreline is shown in figure 1, along with the mean flow for a uniform inlet Mach number $U_\infty = 0.5$. The duct geometry is defined in terms of the lateral offset of the centreline, $y^*$, from its position at the intake $s^* = 0$, with

$$y^*(s^*) = -\frac{h^*}{2}\left(1 - \cos\left(\frac{\pi s^*}{L^*}\right)\right) , \tag{4}$$

The lateral offset at the downstream exit $(s^* = L^*)$ is then $-h^*$. The duct radius varies quartically between upstream (radius $\ell^*$) and downstream (radius $a_f^*$) as

$$\frac{a^*(s^*) - \ell^*}{a_f^* - \ell^*} = 3\left(1 - \frac{s^*}{L^*}\right)^4 - 4\left(1 - \frac{s^*}{L^*}\right)^3 + 1 .$$

For the RAE 2129 duct, $L^*/\ell^* = 7.1$, $h^*/L^* = 0.3$ and $(a_f^*/\ell^*)^2 = 1.4$. This leads to a value of $\varepsilon$ based on the duct length of $\varepsilon = 1/7.1$, for which it is reasonable to suppose that the small-$\varepsilon$ asymptotics of this paper will work well.

## B. Unsteady flow

Consider a small time-dependent perturbation $(\boldsymbol{u}, \rho, p)$ with time dependence $\exp\{\mathrm{i}\omega t\}$ to the mean flow $(\boldsymbol{U}, D, P)$. Introducing a scalar potential $\boldsymbol{u} = \boldsymbol{\nabla}\phi$, and neglecting vortical and entropic perturbations, the equations for the unsteady linearized flow[4] reduce to

$$\frac{\mathrm{D}}{\mathrm{D}t}\left(\frac{1}{C^2}\frac{\mathrm{D}\phi}{\mathrm{D}t}\right) - \frac{1}{D}\boldsymbol{\nabla}\cdot\left(D\boldsymbol{\nabla}\phi\right) = 0, \qquad\qquad p = C^2\rho = -D\frac{\mathrm{D}\phi}{\mathrm{D}t}, \tag{5}$$

where $\mathrm{D}/\mathrm{D}t = \mathrm{i}\omega + \boldsymbol{U}\cdot\boldsymbol{\nabla}$ is the convective derivative with respect to the mean flow. This equation is to be solved subject to the usual hard-wall boundary condition $\partial\phi/\partial r = 0$ at $r = a$. We pose the multiple scales WKB ansatz[5]

$$\phi = \left[A_0(S, r, \theta) + \varepsilon A_1(S, r, \theta) + O(\varepsilon^2)\right]\exp\left\{\mathrm{i}\omega t - \frac{\mathrm{i}}{\varepsilon}\int_0^S k(S')\,dS'\right\} .$$
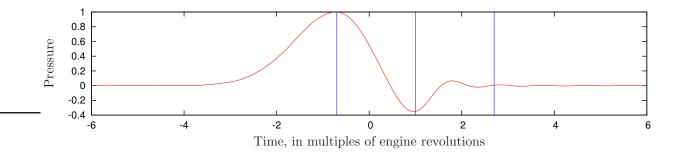
**Figure 2.** The pressure difference from steady state, introduced as a plane wave at the fan face. The vertical lines show the times of the snapshots in figures 3–5.

Substituting this into (5) and taking just the $O(1)$ terms then leads to

$$\frac{1}{h_s D_0}\left[\frac{1}{r}\frac{\partial}{\partial r}\left(rh_s D_0 \frac{\partial A_0}{\partial r}\right) + \frac{1}{r^2}\frac{\partial}{\partial \theta}\left(h_s D_0 \frac{\partial A_0}{\partial \theta}\right)\right] + \left(\frac{\Lambda^2}{C_0{}^2} - \frac{k^2}{h_s{}^2}\right)A_0 = 0 , \tag{6}$$

where $\Lambda = \omega - kU_0/h_s$. The $O(1)$ boundary condition is $\partial A_0/\partial r = 0$. This is solved numerically using a pseudospectral method[1] to determine the axial wavenumber $k(S)$ and the corresponding wave function $A_0(S, r, \theta)$. The amplitude of $A_0$ must be determined from the solvability condition obtained using the $O(\varepsilon)$ terms from (5). By multiplying the $O(\varepsilon)$ part of (5) by $h_s D_0 A_0$, integrating across the duct cross section, and applying the mean flow equations of motion to eliminate $V_1$ and $W_1$, we arrive, after a very considerable amount of algebra, at the requirement

$$\frac{\mathrm{d}}{\mathrm{d}S}\left[\int_0^{2\pi}\int_0^a D_0 A_0^2 \left[\frac{\omega U_0}{C_0{}^2} + \frac{k}{h_s}\left(1 - \frac{U_0{}^2}{C_0{}^2}\right)\right]r\,\mathrm{d}r\,\mathrm{d}\theta\right] = 0 . \tag{7}$$

For cuton modes, this can be interpreted as conservation of energy.

## III.  Wave pulses in the time domain

All the derivation above has been at a single fixed frequency. By taking a periodic signal and decomposing it into its frequency components, each of these frequencies may be analysed as above, and then summed to give a time-domain solution for the propagation of that signal through a curved duct. As an example, consider the pressure signal given in figure 2. This signal has been proposed[a] as being representative of the pressure at the engine fanface for a surge event. Note that the time axis has been given in terms of the number of engine revolutions, as this is how the surge signal is thought to scale. A surge event is a strong pressure disturbance that breaks the linearized small disturbance assumptions of the derivation above. The surge signal is used here to demonstrate the time-domain synthesis from the frequency-domain analysis above, as it is a less artificial signal than a purely hypothetical pulse.

The surge signal is initiated in a straight section of duct as a plane-wave that does not vary across the duct cross-section. This straight section of duct is then smoothly curved to fit onto the downstream end of the RAE 2129 intake, and the upstream end of the RAE 2129 intake is similarly connected to a section of duct that smoothly curves to become straight again. This is so that both ends of the duct are straight and the curvature varies smoothly along the duct. These extra duct sections are given in terms of their lateral offset $y(s)$. They are required to satisfy $y(0) = y'(0) = 0$ to fit smoothly onto the RAE 2129 intake, and $y''(0) = \kappa_0$ and $y''(d) = 0$ to smoothly vary the curvature from $\kappa_0$ to zero over a distance $d$. Here, $d = L/8$ is chosen, and the function used is

$$y(s) = \kappa_0 \left(\frac{1}{2}s^2 - \frac{1}{6d}s^3\right). \tag{8}$$

The propagation of a surge pulse through this modified RAE 2129 intake, with a nondimensionalized engine blade-tip speed of unity, is shown in figures 3–5[b].  These figures plot the pressure difference from

---

[a]Dr J. Longley, University of Cambridge, private communication, 2006.

[b]An animation of this is available from `http://www.damtp.cam.ac.uk/user/ejb48/files/curved_duct_pulse_640x480.mpg` and `http://www.damtp.cam.ac.uk/user/ejb48/files/curved_duct_pulse_1280x1024.mpg`
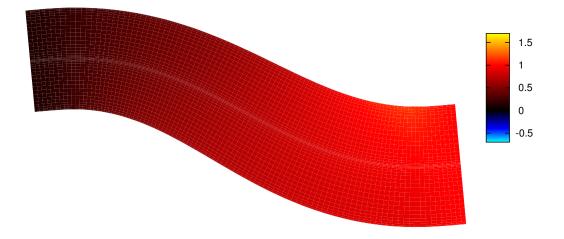
**Figure 3.** The pressure difference from steady state at time $t = -0.7$. The maximum overpressure is just entering the intake from the right.
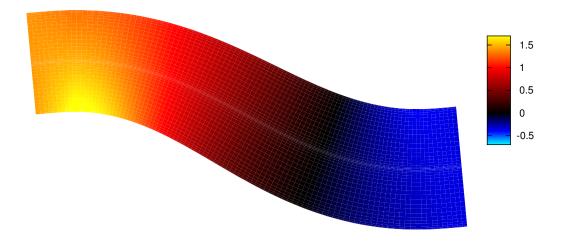


**Figure 4.** The pressure difference from steady state at time $t = 1.0$. The curvature has amplified the pressure on the inside of the left-most bend. The maximum underpressure is just entering the intake from the right.
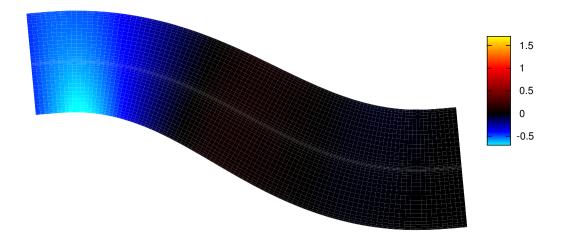


**Figure 5.** The pressure difference from steady state at time $t = 2.7$. The curvature has amplified the underpressure on the inside of the left-most bend.
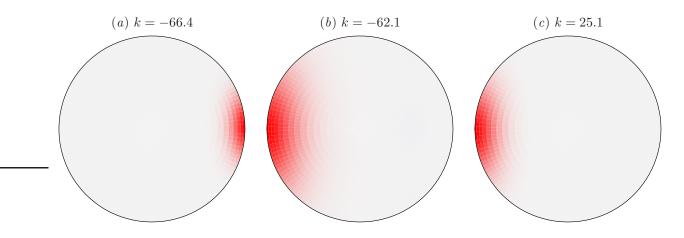
(a) $k = -66.4$  (b) $k = -62.1$  (c) $k = 25.1$

**Figure 6. Curved-duct equivalents of the plane-wave mode, for $\kappa = 0.2$, $U_\infty = 0.5$, and $\omega = 31$. The inside of the bend is on the right. (a) and (b) are upstream-propagating modes, while (c) is a downstream-propagating mode.**

steady state. As can be seen from figure 4, the curvature and narrowing of the intake cause a peak pressure on the intake wall of 1.6 times the peak pressure at the fan face. This peak pressure is highly localized on the inside of the bend closest to the intake lip. The peak underpressure also occurs at the same position, as shown in figure 5, and reaches $-0.6$, while the peak underpressure at the fan face was only $-0.4$.

## IV. Plane wave localization

In the previous section, an upstream-propagating plane-wave mode is seen to be localized on the inside of the duct bend. This is in line with our previous examples,[1] which show the upstream-propagating plane-wave equivalent mode being localized on the inside of the bend and the downstream-propagating mode being localized on the outside. However, this need not always be the case. For example, figure 6 shows that, for $\kappa = 0.2$, $U_\infty = 0.5$, and $\omega = 31$ there are two upstream-propagating fundamental modes, one localized on the inside of the bend and one on the outside, with the downstream-propagating mode still localized on the outside. The wavenumbers for these modes are shown in figure 7, together with a left–right weighting

$$W_x = \frac{\int_0^{2\pi} \int_0^a r \cos(\theta) |A_0(r,\theta)|^2 \, r dr d\theta}{\int_0^{2\pi} \int_0^a |A_0(r,\theta)|^2 \, r dr d\theta}.$$

Modes which are highly localized on the left/right of the duct (i.e. on the outside/inside of the bend) have a value of $W_x$ close to $\mp 1$ respectively. The presence of a couple of upstream modes localized on the outside is clear in figure 7. The question is, therefore, what parameters influence the localization of duct modes? In this section, we investigate this using a raytracing approximation.

### A. Raytracing approximation

In what follows, $S$ will only occur as a parameter specifying which slice of the duct is being considered, and dependence on $S$ will not be explicitly mentioned. The gradient $\nabla_\perp$ is used for the derivative in the cross-section of the duct, i.e. the $r$ and $\theta$ directions only. We start off by introducing the ray ansatz for $A_0(r,\theta)$ by writing

$$A_0(r,\theta) = \frac{\mathcal{A}_0(r,\theta)}{\sqrt{h_s(r,\theta) D_0(r,\theta)}} \exp(-i\omega\psi(r,\theta)) . \tag{9}$$

We will suppose that $\omega$, the dimensionless frequency, is large, so that (9) corresponds to highly oscillatory modes, while both $\psi$ and $\mathcal{A}_0$ are $O(1)$. The corresponding unknown axial eigenvalue will be $O(\omega)$, and so we write $k = \mu\omega$ with $\mu = O(1)$. If we now substitute (9) into (6) and take just the leading terms in $\omega$, i.e.
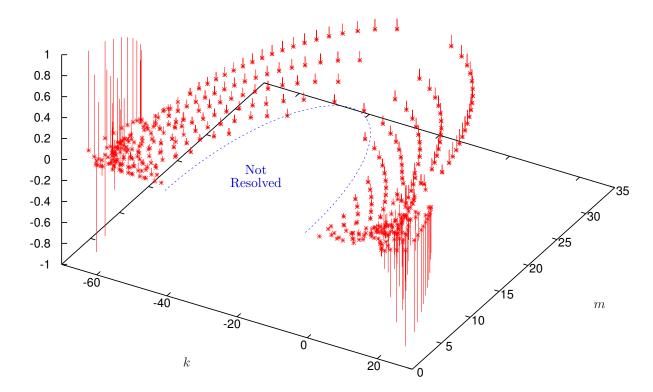
**Figure 7.** The wavenumbers $k$ for propagating modes against their approximate azimuthal order $m$, for $\kappa = 0.2$, $U_\infty = 0.5$, and $\omega = 31$. The vertical axis plots $W_x$, with modes localized on the inside and outside have stalks extending upwards and downwards respectively. Only numerically resolved modes are shown ($n_r = 23$, $n_\theta = 131$); the curve denotes the unresolved region.

$O(\omega^2)$, we find that

$$(\boldsymbol{\nabla}_\perp \psi)^2 = \alpha^2 \, , \qquad \alpha^2 = \frac{1}{C_0{}^2} - \frac{2\mu U_0}{h_s C_0{}^2} - \frac{\mu^2}{h_s{}^2}\left(1 - \frac{U_0{}^2}{C_0{}^2}\right) \, , \tag{10}$$

which is the standard raytracing result for propagation through a medium with nonuniform wavespeed $1/\alpha$. To leading order in $\omega$, the boundary condition simply becomes normal reflection of a ray by the boundary.

## B.  Plane wave localization

In three dimensions, the fundamental modes may be thought of as travelling nearly axially down the duct, reflecting occasionally from the duct boundary. In order to do this, the flow and the geometry must be such that a ray, having just reflected from the boundary, is driven back towards the boundary, as shown in figure 8($a$). Figure 8($b$) shows the corresponding projection of the rays onto the duct cross-section, as derived above. The dashed lines are where $\alpha^2$ becomes negative, the rays being restricted to regions where $\alpha^2$ is positive.

A ray travelling purely axially at the local speed of sound along the duct at a fixed horizontal offset $x$ from the duct centreline would give the raytracing parameter $\mu_\pm(x) = h_s/(U_0 \pm C_0)$, with $+$ for downstream and $-$ for upstream. Substituting $\mu_\pm(x)$ into (10) shows that $\alpha^2 = 0$, corresponding to the fact that such a ray is travelling completely in the axial direction, and therefore has no motion in the duct cross-section. Here, we are concerned with modes localized on the inside or outside boundary, and so (normalizing such that the duct radius is $a = 1$), we are concerned only with the value of $\mu_\pm(x)$ at $x = 1$ (for the inside of the bend) and $x = -1$ (for the outside of the bend). Figure 9 shows the variation of $\alpha^2$ across the duct for the four cases in which $\mu$ takes one of the values $\mu_+(\pm 1)$, $\mu_-(\pm 1)$. Figure 9($b$) corresponds to the parameters used for our previous results,[1] while figure 9($d$) corresponds to figure 6. By perturbing the value of $\mu$ slightly from the values $\mu_\pm(\pm 1)$, it is possible that a small pocket of positive $\alpha^2$ might be created close to the duct wall, and thus (provided the frequency is high enough) a localized mode on that boundary is

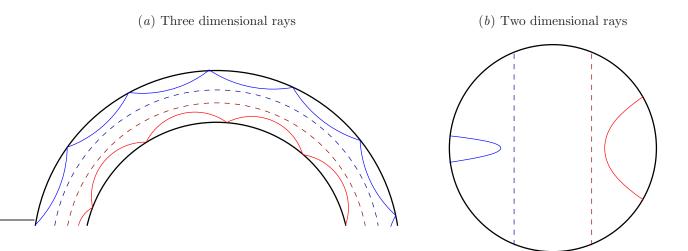(a) Three dimensional rays        (b) Two dimensional rays

**Figure 8. Schematic of localized fundamental rays. The dashed lines are where $\alpha^2 = 0$. (a) shows a projection of the three-dimensional rays onto a vertical plane, and (b) the corresponding projection onto the cross-sectional plane.**

possible. In order for a small perturbation to $\mu$ to lead to a localised mode on the boundary, $\alpha^2(x)$ must decrease away from that boundary. This is also the requirement that a ray having just reflected from the boundary is driven back towards the boundary (it is a standard raytracing result that rays bend towards regions with larger $\alpha$, as may be seen by taking $\nabla_\perp$ of the left hand side of equation 10). A change in the number of localized fundamental modes is therefore seen when the derivative of $\alpha^2$ at $x = \pm 1$ changes sign. As an example, figure 9(a) demonstrates the possibility of a downstream fundamental mode localized on the outside of the bend and an upstream fundamental mode localized on the inside. Figure 9(c) demonstrates the possibility of both the downstream and upstream fundamental modes being localized on the outside of the bend. Figures 9(b,d) both demonstrate the possibility of a downstream fundamental mode localized on the outside, and two upstream fundamental modes, one localized on the inside and one on the outside. Note, however, that for the upstream-propagating outside mode on the outside wall in figure 9(b), the derivative of $\alpha^2$ is very close to zero, implying that a very high frequency would be needed to discover such a mode; this is why such a mode was not seen in our previous results.[1]

In order to investigate which values of $U_\infty$ and $\kappa$ give rise to which types of localization behaviour, we will now look for a change in derivative of $\alpha^2$ at $x = \pm 1$. Differentiating $\alpha^2$ with respect to $x$ and substituting $\mu = \mu_\pm(x) = h_s/(U_0 \pm C_0)$ gives, after some algebraic manipulation,

$$U_0{}^2 = H\left(1 \pm \sqrt{\frac{2}{\gamma+1}}\right). \tag{11}$$

Note that the $+$ solution of this (corresponding to a downstream-propagating mode) is very close to $U_0{}^2 = 2H$, at which point the mean density on the inside of the bend becomes zero. Equation (11) may be evaluated to give $\kappa$ in terms of $U_\infty$, or $U_\infty$ in terms of $\kappa$, for the critical parameters for which an upstream or downstream propagating mode ($-$ or $+$ in equation 11) may be localized on the inside or outside of a bend (evaluating equation 11 at $x = 1$ or $x = -1$). Unfortunately, since $U_\dagger$ depends on both $\kappa$ and $U_\infty$ and is calculated numerically, (11) must in general be solved numerically. However, if the duct cross-sectional area is the same as far upstream, then it can be shown from (3) that $U_\dagger = U_\infty + O(\kappa^2)$. Hence, if the cross-sectional area is the same as far upstream and $\kappa$ is small, (11) gives

$$\kappa = \frac{1}{x}\left(1 - U_\infty\left[H\left(1 \pm \sqrt{\frac{2}{\gamma+1}}\right)\right]^{-1/2}\right), \tag{12}$$

with $x$ being either $+1$ or $-1$ for the inside or outside of the bend, were $H$ is given by (1).

Figure 10 plots the small-curvature asymptotics given by (12) and the numerically calculated solutions of (11), assuming the duct radius is the same as far upstream ($a = 1$). The numerically generated solutions
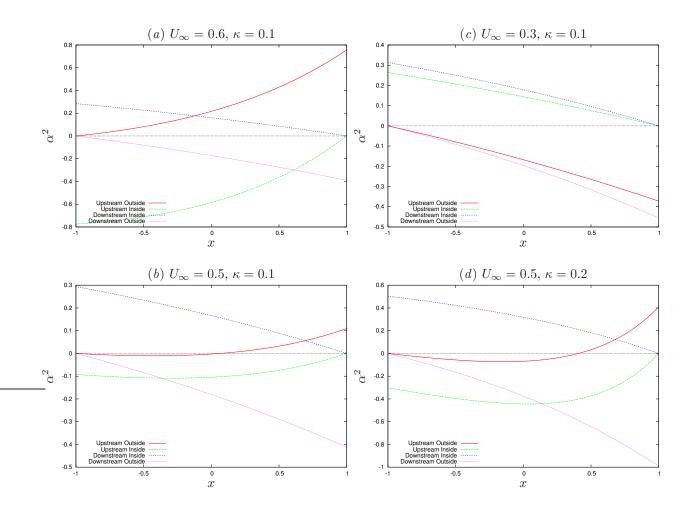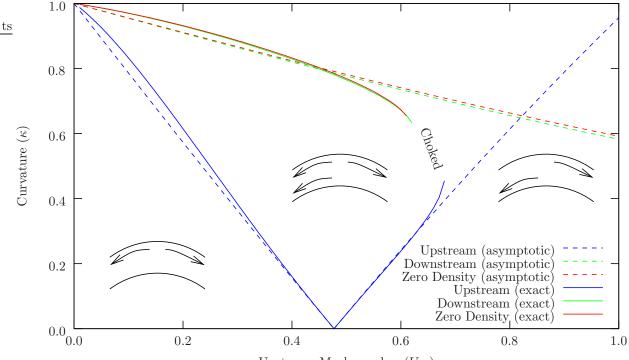
**Figure 9.** Graphs showing the variation in $\alpha^2(x)$ **across the duct cross-section, for potential upstream- and downstream-propagating modes localized on the inside and outside of the duct bend. The solid line is the upstream outside mode (i.e.** $\mu = \mu_-(-1)$)**, the long dashed line the upstream inside (i.e.** $\mu = \mu_-(1)$)**, the short dashed line the downstream inside (i.e.** $\mu = \mu_+(-1)$)**, and the dash-dot line the downstream outside (i.e.** $\mu = \mu_+(1)$)**.**

stop around $U_\infty = 0.65$, since for these parameters the duct is choked; that is, there is no solution to (3) for $U_\dagger$ that gives the required mass flow rate. For low Mach number flows, the geometry keeps both upstream and downstream modes localized on the outside of the bend. This is exactly the result seen by Felix & Pagneux.[6] However, different behaviour is seen for larger Mach number flows. For large Mach number flows, the mean flow is fastest on the inside of the bend and slowest on the outside, giving a refraction effect which curves upstream-propagating rays towards the inside of the bend and downstream-propagating rays towards the outside. Hence, as the Mach number is increased from zero, the upstream mode first becomes present on the inner wall, and then disappears from the outside as the Mach number is increased further. Increasing the curvature makes this effect more pronounced. This case is possibly similar to the unsteady flow through a loaded cascade,[7] in which upstream propagating waves can propagate along the suction surface of the blade (corresponding to the inside of our bend) and become blocked if the mean flow becomes locally close to sonic, giving increased local amplitudes on the suction surface.

While figure 10 is for a duct with the same cross-section as far upstream, (11) is still valid even if this is not the case. The small-$\kappa$ asymptotics of (12) do require this restriction, however. It should also be emphasized that these results, being based on a raytracing approximation, are only valid provided $\omega$ is sufficiently large. Presumably, as the boundary between different behaviour is approached, the frequency necessary for these results to be valid will become large.

American Institute of Aeronautics and Astronautics Paper 2007-3552

**Figure 10. The different localization behaviours of plane waves for different upstream Mach numbers ($U_\infty$) and curvatures ($\kappa$). The sketches show whether upstream and downstream modes localized on the inside and outside of the intake are possible, with downstream being the right-facing arrow. Solid lines are numerical results from (11), and dashed lines are asymptotic results from (12). The two zero-density lines (one numerical and one asymptotic) are where $U_0{}^2 = 2H$, for which the density on the inside of the bend becomes zero.**

## V.    Preliminary nonlinear results

The time-domain signal shown in figure 2 is typically of large amplitude. In order to begin investigating this, we have implemented a two-dimensional inviscid compressible shock-capturing first-order-accurate Godunov numerical scheme.[8] This has been applied to a two-dimensional version of the RAE 2129 intake, with (8) used to smoothly vary the curvature back to zero, just as it was in figures 3–5. Straight sections of intake and exhaust have also been added, to minimise the effect of the inflow and outflow boundary conditions at the edges of the computational domain. The numerical scheme is quick to compute, requiring a total of about 12 CPU hours to give all the results used here.

Initially, the duct is filled with fluid of uniform density, pressure, and velocity, which is then allowed to converge to a steady state. The inflow boundary condition prescribes a constant stagnation pressure and temperature, while the outflow boundary condition of a fixed static pressure is tuned to drive the flow at a prescribed upstream Mach number. The inflow boundary condition is then changed to a nonreflecting one, and the outflow static pressure is varied to give pressure pulse shown in figure 2.

In figures 11–13[c], an upstream Mach number of $U_\infty = 0.5$ is prescribed, and the surge in figure 2 is scaled to give a peak overpressure ratio of 2, implying a peak underpressure of about 0.6. While the imposed pressure profile is smooth, the overpressure shocks midway through the intake, and the underpressure shocks almost immediately on entering the duct. The notable feature of figures 11–13 is that the shock front remains planar, and although the front is not always normal to the duct centreline, nonetheless it exits the curved section as a plane shock without any reflection or mutation due to the curved section. This suggests that a one-dimensional mathematical model may exist, similar in nature to the classical shock-tube theory,[9] that captures the effects of curvature and the corresponding nonsymmetric distribution of pressure over the intake walls. This is currently work in progress.

---

[c]An animation of this is available from `http://www.damtp.cam.ac.uk/user/ejb48/files/nonlinear_pulse.mpg`
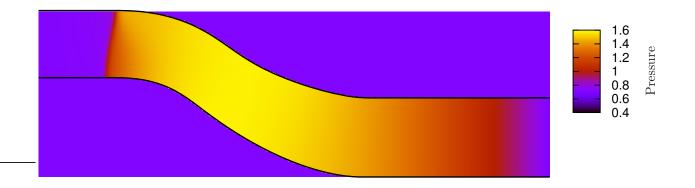
**Figure 11.** The surge pulse shocks midway through the curved section, but remains roughly planar.
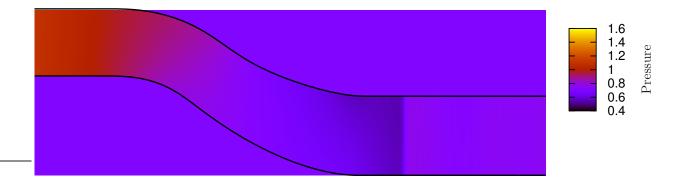


**Figure 12.** The overpressure shock has propagated upstream out of the duct. The underpressure has just entered the duct, and has shocked almost immediately.
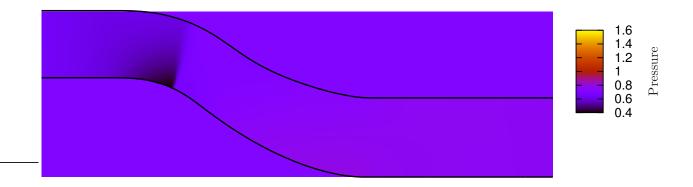


**Figure 13.** The underpressure shock also remains roughly planar.

American Institute of Aeronautics and Astronautics Paper 2007-3552

# VI.    Conclusion

The Multiple Scales approximation for linear time-dependent disturbances in a slowly varying duct with mean flow was first given last year.[1] Here, we have investigated further the less general case of a hollow (as opposed to annular) duct with rigid (as opposed to lined) walls. In the time domain, the significance of curvature is easily seen, with a localized amplification of pressure on the inside of a duct bend by a factor of 1.6 in the example given in figures 3–5. Such plane-wave modes have been investigated further in the high-frequency regime using a raytracing approximation, and an interesting pattern of localization has been found, caused by the competition between curved geometry and refraction effects of the mean flow.

Finally, we presented some preliminary results looking at nonlinear effects in a two-dimensional duct. The results suggest that a one-dimensional mathematical model of nonlinear plane-wave propagation in a curved duct is possible, and should be able to predict, at least qualitatively, the effects of curvature and varying duct diameter on the force exerted on the duct wall during a surge event in a curved aeroengine intake. This is currently work in progress.

## References

[1]Brambley, E. J. and Peake, N., "Sound Transmission in Strongly-Curved Slowly-Varying Cylindrical and Annular Lined Ducts with Flow," No. 2006-2582 in AIAA Paper, 2006.

[2]Rienstra, S. W., "Sound Transmission in Slowly Varying Circular and Annular Lined Ducts with Flow," *J. Fluid Mech.*, Vol. 380, 1999, pp. 279–296.

[3]Menzies, R. D. D., *Investigation of S-Shaped Intake Aerodynamics using Computational Fluid Dynamics*, Ph.D. thesis, University of Glasgow, 2002.

[4]Goldstein, M. E., "Unsteady Vortical and Entropic Distortions of Potential Flows Round Arbitrary Obstacles," *J. Fluid Mech.*, Vol. 89, 1978, pp. 433–468.

[5]Hinch, E. J., *Perurbation Methods*, chap. 7, Cambridge, 1991.

[6]Felix, S. and Pagneux, V., "Sound Attenuation in Lined Bends," *J. Acoust. Soc. Am.*, Vol. 116, 2004, pp. 1921–1931.

[7]Atassi, H. M., Fang, J., and Patrick, S., "Direct Calculation of Sound Radiated from Bodies in Nonuniform Flow," *J. Fluid Eng.*, Vol. 115, 1993, pp. 573–579.

[8]Ben-Artzi, M. and Falcovitz, J., *Generalized Riemann Problems in Computational Fluid Dynamics*, chap. 3 and app. C, Cambridge, 2003.

[9]Lighthill, M. J., *Waves in Fluids*, chap. 2.8–2.10, Cambridge, 1978.